



# Judd–Ofelt and luminescence properties of Dysprosium and Terbium doped bismuth-borate glass system

Asmaa Ratep<sup>1</sup> · Ismail Kashif<sup>2</sup>

Received: 24 October 2022 / Accepted: 28 February 2023 / Published online: 2 May 2023  
© The Author(s) 2023

## Abstract

Absorption spectra of Tb<sup>3+</sup> ions from the ground state <sup>7</sup>F<sub>6</sub> revealed three absorption bands. In addition to the six absorption bands for Dy<sup>3+</sup> ions observed in the visible and near-infrared ranges. The optical band gap of sample free from Dy<sub>2</sub>O<sub>3</sub> (4 mol% Tb<sub>4</sub>O<sub>7</sub>) smaller than other samples containing Dy<sub>2</sub>O<sub>3</sub>. The oscillator strengths and Judd–Ofelt parameters ( $\Omega_2$ ,  $\Omega_4$ ,  $\Omega_6$ ) for reported Dy<sup>3+</sup> and Tb<sup>3+</sup> absorption transitions are estimated, and they do not follow a same trend depend on the substitution between Dy and Tb. The photoluminescence excitation of the Dy<sup>3+</sup> at  $\lambda_{em}=575$  nm reveals the presence of a Tb<sup>3+</sup> peak at 375 nm. The emission spectra of the glasses show that only the  $\lambda_{em}=575$  nm increases due to the excitation of the Tb<sup>3+</sup> at  $\lambda_{em}=545$  nm, indicating effective energy transfer (ET) from the Tb<sup>3+</sup> to Dy<sup>3+</sup> in sample containing Dy<sub>2</sub>O<sub>3</sub> up to 2 mol% and then changed from the Dy<sup>3+</sup> to Tb<sup>3+</sup>. An efficient yellow luminescence arises from the activator's emitting centers. ET predicts the sensitizer's luminescence degradation and the activator's luminescence growth. The color coordinates and the correlated color temperature (CCT) indicate that the glass samples are suitable for white, yellow-green, and blue-light emission depend on the energy of excitation.

**Keywords** Oxide glass · Luminescence · Optical properties · FTIR · X-ray diffraction (XRD) · Judd–Ofelt theory · White LED

## 1 Introduction

The scientific community plays a vital role in increasing color rendering and service life and eliminating the use of traditional incandescent and fluorescent lamps (Ravita and Rao 2021). The W-LED draws attention to the fact that it is not limited in the light it emits by the liquid crystal found in phone and digital camera manufacturing (Sun et al.

---

✉ Asmaa Ratep  
assmakalifa@yahoo.com; asmaa.ratep@women.asu.edu.eg

Ismail Kashif  
ismailkashif52@yahoo.com; ismailkashif@azhar.edu.eg

<sup>1</sup> Department of Physics, Faculty of Women for Art, Science & Education, Ain Shams University, Heliopolis, Cairo, Egypt

<sup>2</sup> Department of Physics, Faculty of Science, Al-Azhar University, Nasr City, Cairo, Egypt

2010), which is characterized by a low luminous flux. Efforts direct to increasing brightness and output at high power.

The W-LED starts as a coating layer of InGaN Blue LED with yellow phosphor emission, followed by the other approach, which is the encapsulation of two or three different types of red, green, and blue emitted phosphors under the excitation of a blue UV lamp (Sun et al. 2010; Wang et al. 2020).

Rare-earth ions are attracting more attention due to their multiple energy levels (Rani et al. 2019), which are suitable for excellent fluorescence in the infrared, visible, and ultraviolet spectral regions.

Bismuth borate glass (Ma et al. 2020) is a good former characterized by the low melting temperature and is formed from various structural units but has high phonon energy.

Overcoming the high phonon energy by adding heavy transition metals (Gökçe and Koçyiğit 2019; Quang et al. 2020; Babu and Cole 2018) enhances the radiative transition probability and improves the luminescence quantum efficiency (Gökçe and Koçyiğit 2019).

Among the many rare-earth ions, choose Dy or Tb because they are generally emitted in the blue-green range. Dy ions emit especially in the visible region. Y/B ratio identifies the covalency around Dy as it achieves white light emission from glass materials (Rani et al. 2019).

Several researchers are studying the effect of Dy doping in different glass formers (Kashif and Ratep 2022a, b; Ichoja et al. 2020; Zhang et al. 2020; Aljewaw et al. 2020; Zaman et al. 2021; Karki et al. 2019; Selvi et al. 2014; Swapna et al. 2013; Rao et al. 2013).

Tb choosing as it emits in the green region ( ${}^5D_4 \rightarrow {}^7F_3$ ) transition, which is suitable for the human eye. Silicon direct coupling detectors are also suitable for many applications, such as lasers, biomedical fields, neutron detection, and w-LED (Kaur et al. 2018; Ramachari et al. 2014). Studies carried out on Tb doped with different formers, Guo et al. (2016) studied optical band gap and photoluminescence in heavily Tb<sup>3+</sup> doped GeO<sub>2</sub>-B<sub>2</sub>O<sub>3</sub>-SiO<sub>2</sub>-Ga<sub>2</sub>O<sub>3</sub> magneto-optical glasses.

Sales et al. (2019) studied concentration-dependent luminescence and energy transfer by relaxation in Tb<sup>3+</sup> fluoroborate-doped glasses.

Glass samples doped with Tb and Dy ions can use to increase the intensity of green emission as Dy is used as a sensitizer for Tb formed by the Dy level ( ${}^4F_{9/2}$ ) populated Tb<sup>3+</sup> level ( ${}^5D_4$ ), and energy transfer happens between these two ions (Ravita and Rao 2021). The low and proximity energy level Dy ( ${}^4F_{9/2}$ ) of Tb ( ${}^5D_4$ ) around 400 cm<sup>-1</sup> allows Dy to become sensitized and transfer energy to Tb. There is an increase in green emissions (Ravita and Rao 2021; Pisarska et al. 2014; Dharmiah et al. 2016). Several papers study the effect of doped glass with double RE (Dy and Tb) as (Bashar et al. 2020) studied Optical studies on Tb<sup>3+</sup>: Dy<sup>3+</sup> singly and doubly doped Borosilicate glasses for white light and solid-state lighting applications. Sun et al. (2009) studied the enhancement of Tb<sup>3+</sup> emission by non-radiative energy transfer from Dy<sup>3+</sup> in silicate glass.

Zur et al. (2018) studied the influence of acceptor concentration on crystallization behavior and luminescence properties of lead borate glasses co-doped with Dy<sup>3+</sup> and Tb<sup>3+</sup> ions. Carreira et al. (2019) studied structural and luminescence characterization of a Dy/Tb co-doped borophosphate glass. Ma et al. (2021) studied boosting visible luminescence of Tb<sup>3+</sup>-activated ZBLAN fluoride glasses by Dy<sup>3+</sup> co-doping. Dharmiah et al. (2016) studied luminescence and energy transfer in Dy<sup>3+</sup>/Tb<sup>3+</sup> co-doped transparent oxyfluoro silicate glass-ceramics for green-emitting applications. Kumar and Rao (2021) studied the influence of Tb<sup>3+</sup> ions concentration and temperature on lithium bismuth aluminum borosilicate

glasses for green photonic device applications. Juarez-Batalla et al. (2017) studied green to white tunable light-emitting phosphors: Dy<sup>3+</sup>/Tb<sup>3+</sup> in zinc phosphate glasses.

Ramachari et al. (2014) studied energy transfer and photoluminescence properties of Dy<sup>3+</sup>/Tb<sup>3+</sup> co-doped oxyfluoride silicate glass–ceramics for solid-state white lighting.

Our main goal in the current work is to understand the suitability of the glass samples under anesthetic study using Dy<sup>3+</sup> and Tb<sup>3+</sup> to obtain effective white, green, blue, and red emissions useful for the application of photovoltaic device. The visible emission, age and energy transfer of the glasses were determined using photoluminescence and lifetime decay profiles. The effect of Tb ion substitution at the expense of Dy ions on optical properties and emissions was studied.

## 2 Experimental work

Glass samples with the following compositions: (30 Bi<sub>2</sub>O<sub>3</sub>+30 B<sub>2</sub>O<sub>3</sub>+10 Ga<sub>2</sub>O<sub>3</sub>+10 GeO<sub>2</sub>+10 TeO<sub>2</sub>+10 SiO<sub>2</sub>) (4-X) Dy<sub>2</sub>O<sub>3</sub>+xTb<sub>4</sub>O<sub>7</sub> (where x=0, 1, 2, 3, and 4) mol% were prepared and denoted by 0Tb-4Dy, 1Tb-3Dy, 2Tb-2Dy, 3Tb-1Dy, and 4Tb-0Dy.

The chemical's purity grades were mixed and annealed for 15 min at 400 °C in a porcelain crucible, then melted at 1000 °C in an electric programmable and automatic temperature control oven (Lenton thermal designs of type VAF15/10). The molten material was cooled and poured between two copper plates in the air. All samples are examined using the Philips Analytical X-ray analysis system (type PW3710) with Cu K $\alpha$ =1.54°A.

The density of glasses is determined by the Archimedes method in which the sample is weighed more than once in the air and when immersed in toluene at room temperature. Density calculation uses the formula

$$\rho = \frac{W_a}{(W_a - W_b)} \times 0.865$$

where  $\rho$  is the density of the glass sample,  $W_a$  is the weight of the glass sample in air,  $W_b$  is the weight of the glass sample in toluene, and 0.865 is the density of toluene.

The optical properties of glass samples (transmission, absorption, excitation, emission, and lifetime decay) were measured using a JASCO V-570 spectrophotometer (with a precision of 1 nm) and a JASCO FP-8300 spectrofluorometer (with a 150 W Xenon arc lamp).

## 3 Results and discussion

Figure 1 shows the absence of peaks and the presence of a hump that represents the amorphous nature of glass.

The application of light on a sample doped with RE was mainly affected by the UV–Vis spectrum as each RE has significant transitions from the ground state to the different excited states. Figure 2 shows the UV–Vis-near IR spectra of glass samples, the first addition of Dy<sub>2</sub>O<sub>3</sub> with a concentration of 4 mol% indicates a significant energy level of third ionization of Dy, reported as the transition from <sup>6</sup>H<sub>15/2</sub> (ground state) to <sup>6</sup>H<sub>11/2</sub>, <sup>6</sup>F<sub>11/2</sub>+<sup>6</sup>H<sub>9/2</sub>, <sup>6</sup>F<sub>9/2</sub>, <sup>6</sup>F<sub>7/2</sub>, <sup>6</sup>F<sub>5/2</sub>, <sup>6</sup>F<sub>3/2</sub>, <sup>4</sup>F<sub>9/2</sub>, and <sup>4</sup>I<sub>15/2</sub> at 1696, 1274, 1102, 906, 810, 778, 470 and 458 nm (Babu and Cole 2018; Karki et al. 2019; Shaaban et al.2018; Kashif and Ratep 2022a, b). The hypersensitive transition is sensitive to the ligand environment of

**Fig. 1** X-ray diffraction patterns of glass samples

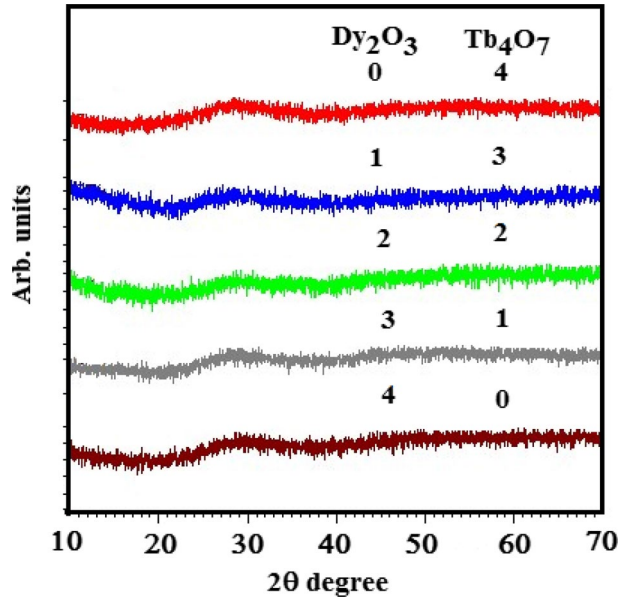
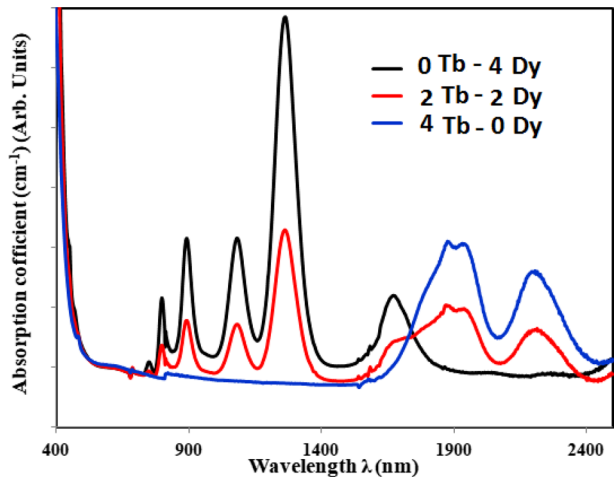


**Fig. 2** the UV–Vis–near IR spectra of glass samples



$\text{Dy}^{3+}$  sites selected at high intensity at 1274 nm and follows the selection rule  $\Delta S=0$ ,  $|\Delta L| \leq 2$ , and  $|\Delta J| \leq 2$  (Babu and Cole 2018; Divina et al. 2021).

The disappearance of peaks below 600 nm reflects the strong absorption of the host matrix under UV illumination (Divina et al. 2021).

A persistent decrease in the concentration of 1 mol% Dy was replaced by 1 mol%  $\text{Tb}_4\text{O}_7$  in each sample, causing the intensity of Dy peaks to decrease.

In addition to the appearance of amplitude peaks in the NIR region characterizing  $\text{Tb}^{3+}$  ions at 2228, 1944, 1898, and 1812, representing the forbidden spin transition from the ground state  ${}^7\text{F}_6$  to the excited states  ${}^7\text{F}_3$  and  ${}^7\text{F}_2$ , the appearance of peaks at UV–Vis 392

and 488 nm represents the  ${}^7F_6 \rightarrow {}^5L_{10} + {}^5G_5$  ( ${}^5D_3$ ) and  ${}^7F_6 \rightarrow {}^5D_4$  ( ${}^5D_4$ ) (Quang et al. 2020; Kumar and Rao 2021; Chen et al. 2017). The appearance of a new band indicates the high solubility of RE (Hegde et al. 2019).

The absorption spectra were used to determine the bonding parameters ( $\delta$ ) of RE with its surrounding ligand by the nephelauxetic ratio ( $\beta$ ) according to the

$$\delta = \frac{1 - \beta'}{\beta'} \times 100 \quad \text{where} \quad \beta' = \frac{\sum \beta}{\text{number of energy level}}$$

where  $\beta = \nu_c/\nu_a$  as  $\nu_c$  is the transition of RE ion in the host matrix,  $\nu_a$  is the aqua ion transition (Table 1).

The value obtained decomposes the type of bond because it is ionic when negative and covalent when positive. The determined values were detected in the negative charge that detected the ionic bond, and the value decreased with the increase of  $Tb_4O_7$  as the trend of bonding was directed to increase the covalency. The interaction of light with electrons in the valance band passing through the band gap to the conduction band decides their suitability in optoelectronics devices (Hegde et al. 2019). In addition to the determination of material type as becoming a semiconductor in the range of 0–4 eV for  $E_g$ , while an insulator at  $E_g > 4$  eV (Shaaban et al. 2018), it is sensitive mainly to the RE addition through the glass preparation.

Based on the relation, Mott and Davis proposed an  $E_g$  determination for direct and indirect allowed and forbidden transitions (Selvi et al. 2014).

$$\alpha(\nu)h\nu = \beta(h\nu - E_g)^n$$

where  $\alpha$  is the absorption coefficient,  $\beta$  is constant, and  $n = 2, 1/2, 3,$  and  $3/2$  is the type of transition (direct, indirect, allowed, and forbidden).

**Table 1** the observed transition of Tb and Dy ions, nephelauxetic ratio and bonding parameters ( $\beta'$  and  $\delta$ ) of glass samples

Transition	$\nu_c$					$\nu_a$ (aqua ion)
	0Tb-4Dy	1Tb-3Dy	2Tb-2Dy	3Tb-1Dy	4Tb-0Dy	
7F6 → 7F3	–	4516	4533	4533	4541	4344
7F6 → 7F2	–	5149	5154	5165	5154.7	5028
7F6 → 7F1	–	5330	5324.9	5324.9	5324.9	5481
7F6 → 7F0	–	–	–	5574	5586	5703
6H15/2 → 6H11/2	5980.9	5966	5952	–	–	5833
6H15/2 → 6F11/2 + 6H9/2	7924	7924	7899	7949	–	7730
6H15/2 → 6F9/2	9259	9259	9191	9259	–	9115
6H15/2 → 6F7/2,	11,186	11,211	11,186	11,186	–	11,025
6H15/2 → 6F5/2	12,531	12,500	12,500	12,500	–	12,432
6H15/2 → 6F3/2	13,298	13,298	13,298	13,333	–	13,212
7F6 → 5D4	–	20,747	20,492	20,661	20,661	20,545
6H15/2 → 4F9/2	22,293	–	–	–	–	21,144
7F6 → 5G6	–	–	–	–	26,316	26,425
$\beta'$	1.021	1.0109	1.0086	1.00701	1.0038	
$\delta$	–0.0209	–0.0108	–0.0085	–0.0069	–0.00383	

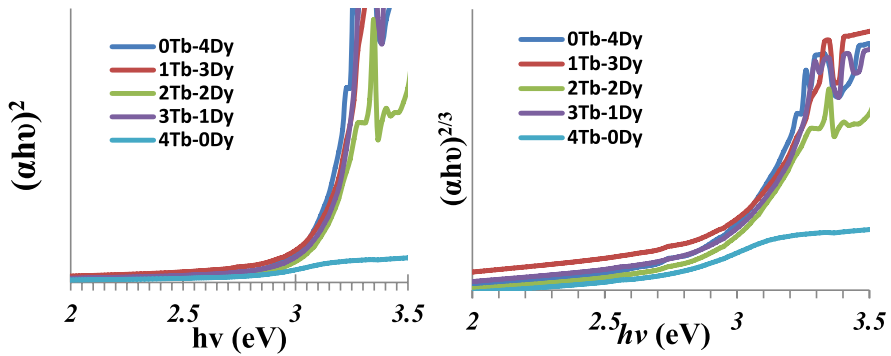


Fig. 3 Tauc plots between  $(\alpha hv)^2$  and  $(\alpha hv)^{2/3}$  besides  $h\nu$  (eV) for glass samples

Table 2 Optical band gap energy for glass samples

Sample	Energy band gap (eV)	
	n=2	n=3/2
0Tb-4Dy	3.1	2.8
1Tb-3Dy	3.15	2.8
2Tb-2Dy	3.07	2.8
3Tb-1Dy	3.15	2.8
4Tb-0Dy	2.75	2.1

Figure 3 represents the best straight line for the relation  $(\alpha hv)^2$  and  $(\alpha hv)^{2/3}$ . Chosen  $n = 1/2$  and  $3/2$  for the calculation and plotting of band gap graph because the tangential line of both  $n = 1/2$  and  $n = 3/2$  passes through the largest number of points, unlike  $n = 2$  and  $n = 3$ , so they were excluded. The  $E_g$  values are calculated by extrapolating the previous relation to a value = 0 at the x-axis. All energy gap values are tabulated in Table 2.

Many researchers (Babu and Cole 2018; Aljewaw et al. 2020; Guo et al. 2016; Kashif and Ratep 2022a, b; Chen et al. 2017) study the effect of adding the RE as Dy or Tb on different glass formers.

Figure 4 shows the density calculated from the Archimedes method represented in two parts. The first part is the former doped with one of the RE, and the other part is the former doped with mixed RE.

In the part of adding one type of RE to glass, it noticed the greater density of  $Tb_4O_7$  glass than  $Dy_2O_3$  glass. The higher density for glass doped with  $Tb_4O_7$  than with  $Dy_2O_3$  is explained by the higher  $MW_t$  (molecular weight) of  $Tb_4O_7$  than with  $Dy_2O_3$ .

The density change is explained by the state of structural compression of the glass that occurs with the addition of different RE and increases with increasing rare-earth content (Babu and Cole 2018; Zaman et al. 2021; Guo et al. 2016; Yang and Zhu 2021; Hegde et al. 2019; Kashif and Ratep 2021).

The probability of transitions between the ground state and different energy levels of rare-earth ions expresses the oscillator strength.

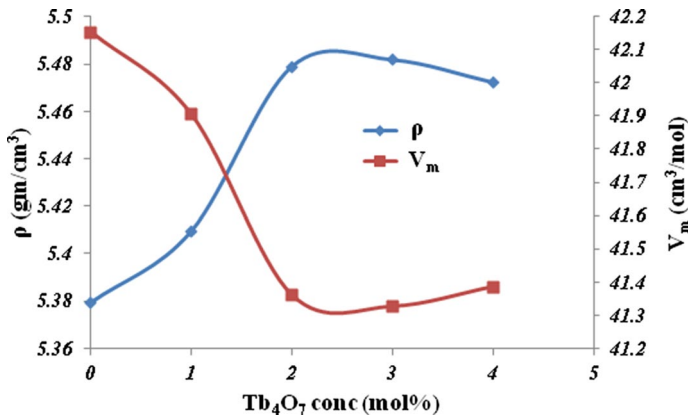


Fig. 4 Relation between the density, molar volume, and Dy<sub>2</sub>O<sub>3</sub> concentration of glass samples

In other words, the oscillator strength is the indicating tool of the absorption intensity measured as the integrated area of the peak, which comprises information about electronic transitions and radiative properties according to the relation

$$f_{\text{exp}} = 4.318 \times 10^{-9} \int \alpha(\nu) d\nu$$

The theoretical method derived by Judd–Ofelt’s theory calculates an electric dipole transition from the ground state  $\Psi J$  to an excited state  $\Psi' J'$  is given by

$$f_{\text{cal}} = \frac{8\pi^2 mc(n^2 + 1)^2}{3h\lambda(2J + 1)9n} \sum_{\lambda=2,4,6} \Omega_{\lambda}(\Psi J \| U^{\lambda} \| \Psi' J')^2$$

The root mean square deviation given by the relation

$$\delta_{\text{rms}} = \left[ \frac{\sum (f_{\text{exp}} - f_{\text{cal}})^2}{N - 3} \right]^{\frac{1}{2}}$$

Examine the quality fit between the experimental and calculated oscillator strength, while the result is present in Table 3.

From the results obtained, noticed the low value, which shows the validity of the Judd–Ofelt (JO) theory and the agreement between the experimental and theoretical oscillator power.

JO parameter determined with the help of  $f_{\text{exp}}$ ,  $f_{\text{cal}}$ , and refractive index using the root mean square fitting approximation procedure gave deep insight about the symmetry/asymmetric bonding and the nature of the bond between the surrounding ligand around RE. The intensity of parameters affects the chemical composition and the symmetry around RE (Divina et al. 2021). The abrupt modification structure around RE (Babu and Cole 2018; Divina et al. 2021) is demonstrated by the fact that the intensity of a parameter changes with any composition change.

The calculated experimental oscillator strengths are a facility where it is calculated for each peak in a separate calculation while the JO parameters are based on the reduced squared matrix element U<sub>2</sub>, 4, 6 values. In samples containing double RE, the bands of

**Table 3** Observed band positions ( $\text{cm}^{-1}$ ), oscillator strength ( $f_{\text{exp}}$  and  $f_{\text{calc}}$ ), Judd–Ofelt parameters ( $\Omega_\lambda \times 10^{-20}$ ), and  $\delta_{\text{rms}} \times 10^{-6}$  of the  $\text{Dy}^{3+}:\text{Tb}^{3+}$  co-doped  $\text{Bi}_2\text{O}_3\text{-B}_2\text{O}_3\text{-Ga}_2\text{O}_3\text{-GeO}_2\text{-TeO}_2\text{-SiO}_2$  glasses

$\lambda$ (nm)	0Tb-4Dy		1Tb-3Dy		2Tb-2Dy		3Tb-1Dy		4Tb-0Dy	
	$f_{\text{exp}}$	$f_{\text{calc}}$	$f_{\text{exp}}$	$f_{\text{calc}}$	$f_{\text{exp}}$	$f_{\text{calc}}$	$f_{\text{exp}}$	$f_{\text{calc}}$	$f_{\text{exp}}$	$f_{\text{calc}}$
2206	–	–	28.5	9.64	35.2	9.11	30.9	6.186	24.2	25.1
1940	–	–	32	5.84	22.3	11.3	15.9	7.80	17.8	14.8
1878	–	–	66.9	3.61	34	9.26	5.48	6.46	3.59	8.99
1786	–	–	–	–	–	–	13.7	2.60	9.72	3.61
1680	12.9	9.93	4.35	7.65	6.55	16.6	–	–	–	–
1266	57.5	5.80	43.7	49.8	45.6	44.3	39.5	10.7	–	–
1088	13.3	1.20	10.6	36.2	12.4	28.1	10.7	19.1	–	–
894	8.19	1.295	5.7	19.2	7.33	30.6	4.85	21.1	–	–
800	3.10	6.85	3.30	6.32	2.12	16.2	2.55	11.3	–	–
752	0.42	1.28	0.3	1.19	0.297	3.04	1.29	2.13	–	–
484	–	–	–	–	–	–	0.617	0.0949	0.696	0.700
470	0.638	3.48	–	–	–	–	–	–	–	–
452	0.857	2.55	–	–	–	–	–	–	–	–
380	–	–	–	–	–	–	–	–	1.68	0.258
$\delta_{\text{rms}}$	4.48	–	22.8	–	11.8	–	5.04	–	2.45	–
$\Omega_2$	5.03E-19	–	1.22E-19	–	2.87E-19	–	1.50E-20	–	8.11E-19	–
$\Omega_4$	1.09E-20	–	3.53E-19	–	2.50E-20	–	8.25E-21	–	8.34E-19	–
$\Omega_6$	1.14E-19	–	1.06E-19	–	2.67E-19	–	1.90E-19	–	2.37E-19	–
$\Omega_4/\Omega_6$	0.095	–	3.32	–	0.093	–	0.043	–	3.52	–

$\text{Tb}^{3+}$  and  $\text{Dy}^{3+}$  separated and not overlapped. We are supposed to sum the two RE peaks in the same calculation. With the increase of Tb concentration, it was observed that the intensity of Dy peaks decreased, and the peak of Tb appeared.

Among the JO parameters,  $\Omega_2$  is the most sensitive to ambient, providing the opportunity to understand the asymmetry around rare-earth ions, the polarization of ligand ions, and the covalency around rare-earth ions.

So, the parameters  $\Omega_4$  and  $\Omega_6$  are less sensitive to the vicinity and can give information about the bulk properties like rigidity and viscosity (Quang et al. 2020).

Figure 5 shows the JO parameters as a function of  $\text{Tb}_4\text{O}_7$  concentration. In general, the  $\Omega_2$  values are larger than  $\Omega_4$  and  $\Omega_6$  except in the sample 3Tb-1Dy which has a lower value of  $\Omega_2$  than  $\Omega_6$ . Higher values of  $\Omega_2$  show a higher covalency and are asymmetric around rare-earth ions (Karki et al. 2019). The greater value of  $\Omega_2$  in samples (0Tb-4Dy), (2Tb-2Dy), and (4Tb-0Dy) led to the highest green luminescence emission at 543 nm (Quang et al. 2020).

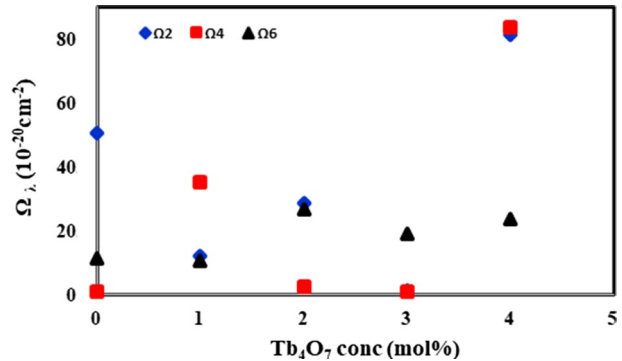
The higher value of  $\Omega_6$  in sample 2Tb-2Dy explains the high polarized around RE, the rigidity (Mariyappan et al. 2016).

The increase in  $\Omega_6$  values over 4 in all samples explains a host effect with rare-earth ions at different concentrations (Divina et al. 2021).

The JO parameters are useful in determining the highest stimulated emission cross-section used in the photonic device (Mariyappan et al. 2016). The Judd–Ofelt parameter intensities values of the glass samples under study are higher than the other glass



**Fig. 5** The Judd–Ofelt parameters of prepared glass samples



systems, suggesting that Dy<sup>3+</sup> and Tb<sup>3+</sup> was successfully doped in the glass matrix, according to Table 4. The samples under study have Ω<sub>2</sub> larger than the other samples which is evidenced by the fact that the samples under study are more suitable for optical applications.

Excitation spectra for glass samples doped with Dy<sub>2</sub>O<sub>3</sub> and Tb<sub>4</sub>O<sub>7</sub> are shown in Fig. 6a and b from monitoring the emission at λ<sub>em</sub> = 575 nm (Dy<sup>3+</sup>) and λ<sub>em</sub> = 545 nm (Tb<sup>3+</sup>) respectively.

The excitation spectrum of sample doped with Dy shown in Fig. 6a, the has six peaks at 353, 367, 383, 428, 454, and 475, corresponding to the 4F–4F transition from the ground state <sup>6</sup>H<sub>15/2</sub> to <sup>6</sup>P<sub>7/2</sub>, <sup>4</sup>P<sub>3/2</sub>, <sup>4</sup>I<sub>13/2</sub>, <sup>4</sup>G<sub>11/2</sub>, <sup>4</sup>I<sub>15/2</sub>, and <sup>4</sup>F<sub>9/2</sub>, respectively (Bahadur et al. 2017).

Figure 6b show that the Tb<sup>3+</sup> excitation spectrum exhibited four peaks at 354, 369, 380, and 486 nm in the Tb<sub>4</sub>O<sub>7</sub> doped sample correspond to the transition from ground state <sup>7</sup>F<sub>6</sub> to various excited states <sup>5</sup>L<sub>9</sub>, <sup>5</sup>G<sub>5</sub>, <sup>5</sup>D<sub>3</sub>, and <sup>5</sup>D<sub>4</sub> (Kaur et al. 2018; Bahadur et al. 2017).

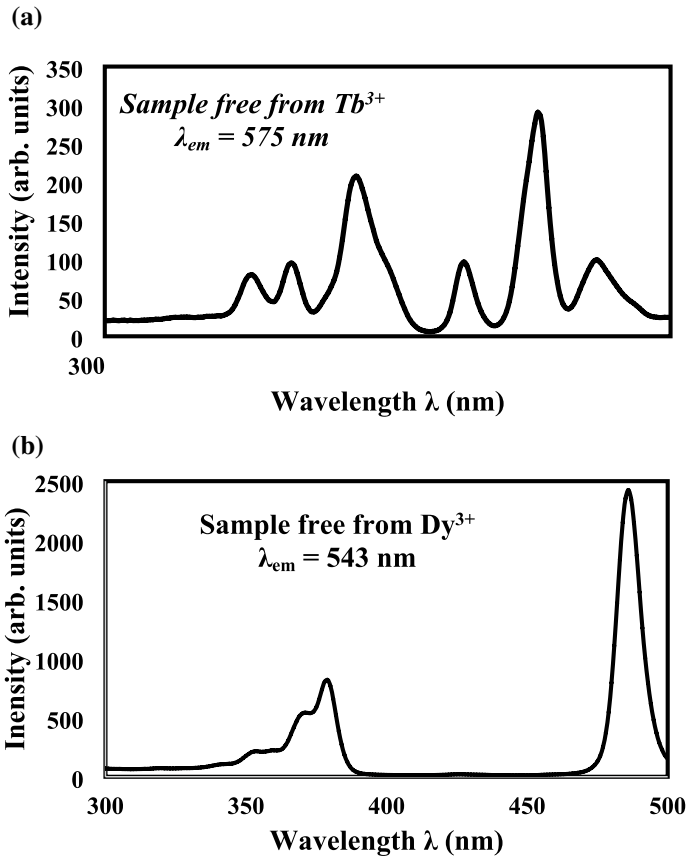
The samples doped with Dy–Tb were recorded by monitoring wavelength at 575 and 545 nm are shown in Fig. 7a and b. From Fig. 7a clear that the excitation peaks representing the Dy transitions like the transition shown in Fig. 6a. There was no significant change in the excitation spectra after adding Tb<sup>3+</sup> ions to glass samples.

The recording of excitation bands due to Dy<sup>3+</sup> ions under Tb<sup>3+</sup> emission wavelength of 545 nm in samples doped with both Dy–Tb indicates the occurrence of energy transmission from Dy<sup>3+</sup> to Tb<sup>3+</sup> ions (Ravita and Rao 2021; Pisarska et al. 2014).

Figure 7a shows the excitation profile of Dy/Tb co-doped glass samples under 575 nm emission wavelength. The excitation spectrum measured at 575 nm exhibits seven peaks six assigned Dy ions at 354, 367, 389, 427, 454, and 474 nm pertaining to the transition of <sup>6</sup>H<sub>15/2</sub> → <sup>6</sup>P<sub>7/2</sub>, <sup>6</sup>P<sub>5/2</sub>, <sup>4</sup>I<sub>13/2</sub>, <sup>4</sup>G<sub>11/2</sub> and <sup>4</sup>F<sub>9/2</sub> respectively. The remaining band at 488 nm corresponding to <sup>7</sup>F<sub>6</sub> → <sup>5</sup>D<sub>4</sub> transition. As shown in Fig. 7b the excitation spectrum recorder under 543 nm emission wavelength of Tb<sup>3+</sup> ions show eight excitation bands; four are assigned to Tb<sup>3+</sup> ion and four bands are assigned to Dy<sup>3+</sup> ions. The bands at 354, 370, 379, and 486 nm corresponding to <sup>6</sup>F<sub>6</sub> → <sup>5</sup>L<sub>9</sub>, <sup>5</sup>L<sub>10</sub>, <sup>5</sup>G<sub>6</sub> and <sup>5</sup>D<sub>4</sub> transition respectively. The four excitation bands due to the Dy<sup>3+</sup> ions observed at 390, 427, 454, and 474 nm. The presence of excitation band due to Tb<sup>3+</sup> ions while recording under Dy<sup>3+</sup> emission wavelength 575 nm and the presence of excitation band due to Dy<sup>3+</sup> ions while recording under Tb<sup>3+</sup> emission wavelength 543 nm indicate the occurrence of energy transmission from Dy<sup>3+</sup> to Tb<sup>3+</sup> (Bashar et al. 2020) and from Tb<sup>3+</sup> to Dy<sup>3+</sup> ions (Ravita and Rao 2021). The excitation peaks are determined in Fig. 7a and b which confirm the ability of samples excited by ultraviolet light (UV), near-ultraviolet light (N-UV), and blue light to excite (Babu and Cole 2018; Kaur et al. 2018).

**Table 4** The previous studies of Judd–Ofelt parameters ( $\Omega\lambda \times 10^{-20}$ )

Glass	$\Omega_2$	$\Omega_4$	$\Omega_6$	Trend	Refs.
$\text{Bi}_2\text{O}_3\text{-B}_2\text{O}_3\text{-Ga}_2\text{O}_3\text{-GeO}_2\text{-TeO}_2\text{-SiO}_2\text{-4Dy}_2\text{O}_3\text{:0Tp}_4\text{O}_7$	50.3	1.09	11.4	$\Omega_2 > \Omega_6 > \Omega_4$	Present work
$\text{Bi}_2\text{O}_3\text{-B}_2\text{O}_3\text{-Ga}_2\text{O}_3\text{-GeO}_2\text{-TeO}_2\text{-SiO}_2\text{-3Dy}_2\text{O}_3\text{:1Tp}_4\text{O}_7$	12.2	35.3	10.6	$\Omega_4 > \Omega_2 > \Omega_6$	P.W.
$\text{Bi}_2\text{O}_3\text{-B}_2\text{O}_3\text{-Ga}_2\text{O}_3\text{-GeO}_2\text{-TeO}_2\text{-SiO}_2\text{-2Dy}_2\text{O}_3\text{:2Tp}_4\text{O}_7$	28.7	2.25	26.7	$\Omega_2 > \Omega_6 > \Omega_4$	P.W.
$\text{Bi}_2\text{O}_3\text{-B}_2\text{O}_3\text{-Ga}_2\text{O}_3\text{-GeO}_2\text{-TeO}_2\text{-SiO}_2\text{-1Dy}_2\text{O}_3\text{:3Tp}_4\text{O}_7$	1.5	0.8	19.0	$\Omega_6 > \Omega_2 > \Omega_4$	P.W.
$\text{Bi}_2\text{O}_3\text{-B}_2\text{O}_3\text{-Ga}_2\text{O}_3\text{-GeO}_2\text{-TeO}_2\text{-SiO}_2\text{-0Dy}_2\text{O}_3\text{:4Tp}_4\text{O}_7$	81.1	83.4	23.7	$\Omega_4 > \Omega_2 > \Omega_6$	P.W.
10BiNFBs	0.272	1.882	2.138	$\Omega_6 > \Omega_4 > \Omega_2$	Mariyappan et al. (2016)
NPABSDy10	14.495	1.264	2.234	$\Omega_2 > \Omega_6 > \Omega_4$	Babu and Cole (2018)
PbFPDy10	7.12	1.59	2.20	$\Omega_2 > \Omega_6 > \Omega_4$	Kesavulu and Jayasankar (2011)
59.5B2O3–10TeO2–10Al2O3–20Li2O–0.5Tb2O3	11.85	5.73	4.42	$\Omega_2 > \Omega_4 > \Omega_6$	Quang et al. (2020)
49.5P2O5–10AlF3–10BaF2–10SF2–10PbO–10Na2O–0.5Dy2O3	20.45	3.15	4.27	$\Omega_2 > \Omega_6 > \Omega_4$	Babu et al. (2015)
40 PbO–5 Al2O3–54SiO2:1.0 Dy2O3	15.7	0.927	2.83	$\Omega_2 > \Omega_6 > \Omega_4$	Rao et al. (2013)
25 MoO3–15 SiO2–20 Dy2O3–40 Na2B4O7	1.11	0.48	1.50	$\Omega_2 > \Omega_6 > \Omega_4$	Shaaban et al. (2018)
1DyNFBT	7.834	1.863	1.987	$\Omega_2 > \Omega_6 > \Omega_4$	Mariselvam and Liu (2021)
LSBP2Dy	5.31	2.12	2.03	$\Omega_2 > \Omega_4 > \Omega_6$	Vijayakumar et al. (2015)
60 B2O3 + 9 ZnO + 10 Al2O3 + 20 Bi2O3 + 1 Dy2O3	12.03	2.33	2.74	$\Omega_2 > \Omega_6 > \Omega_4$	Swapna et al. (2013)
BGGD1.00	3.65	0.65	1.57	$\Omega_2 > \Omega_6 > \Omega_4$	Gökçe and Kocyigit (2019)



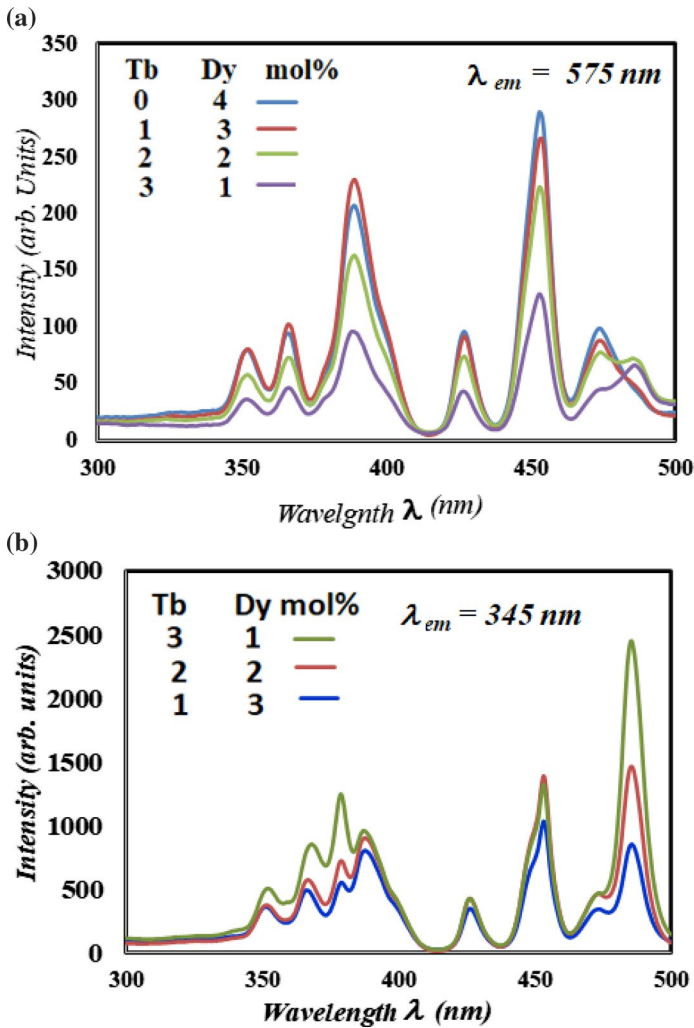
**Fig. 6** **a** The excitation spectra of glass sample free from  $Tb^{3+}$  at 575 nm. **b** The excitation spectra of glass sample free from  $Dy^{3+}$  at 545 nm

Figure 8 shows the emission for the  $Dy^{3+}/Tb^{3+}$  co-doped glass samples under excitation at 351 nm. It consists of six emission peaks: four corresponding to  $Tb^{3+}$  ions and two corresponding to  $Dy^{3+}$  ions. The peaks due  $Tb^{3+}$  are situated at 488, 544, 583 and 621 nm and the peaks due  $Dy^{3+}$  are situated at 475 and 575 nm.

In Fig. 8 conspicuous that, with increase in  $Tb^{3+}$  ion concentration, the intensity of peaks corresponding to  $Tb^{3+}$  (544 nm) continuously increasing up to 2 mol %  $Tb_4O_7$  and then slow decrease. It indicates that this concentration is the best energy transfer condition. And the decrease is demonstrating a reverse energy transfer from  $Tb^{3+}$  to  $Dy^{3+}$  ions (Ma et al 2021).

As shown in Fig. 8, the emission spectra used to calculate the emission parameters coordinate through the CIE 1931 color chromaticity using the color matching function;  $X'(y)$ ;  $Y'(y)$ ; and  $Z'(y)$  as shown in Fig. 9a.

The coordination of glass samples excited at 351 is determined and tabulated in Table 5A. The data obtained explains the appearance of light emission in a different color. Sample 0Tb-4Dy excited at 351 nm (Divina et al. 2021) have a similar standpoint (0.314, 0.301). While the samples doped doubly Tb-Dy and 4Tb-0Dy indicate the greenish color



**Fig. 7** **a** The excitation spectra of glass sample containing  $\text{Dy}^{3+}$  and  $\text{Tb}^{3+}$  at 575 nm. **b** the excitation spectra of glass sample containing  $\text{Dy}^{3+}$  and  $\text{Tb}^{3+}$  at 545 nm

shifted to blue emission, as it may be explained by the ratio between green to yellow (Table 5A), as the increase of the ratio to reach a value larger than 1 contributes to the yellow-green emission.–

The lifetime is important factor for potential laser materials. The fluorescence decay curve of  $\text{Dy}^{3+}$  ion and  $\text{Tb}^{3+}$  excited at 351, 388 and 453 nm and monitored at 575 nm and 543 nm at room temperature of the present samples was measured and is shown in Fig. 9b and c. The decay curves are deviated from single exponential, the decay profile is found to be biexponential for some samples and other follow single exponential decay. The bi-exponential nature may be because of the reason that the energy transfer from excited donor ion to unexcited acceptor ion transpires. The intensity of luminescence can be articulated as follows (Ye et al. 2023):

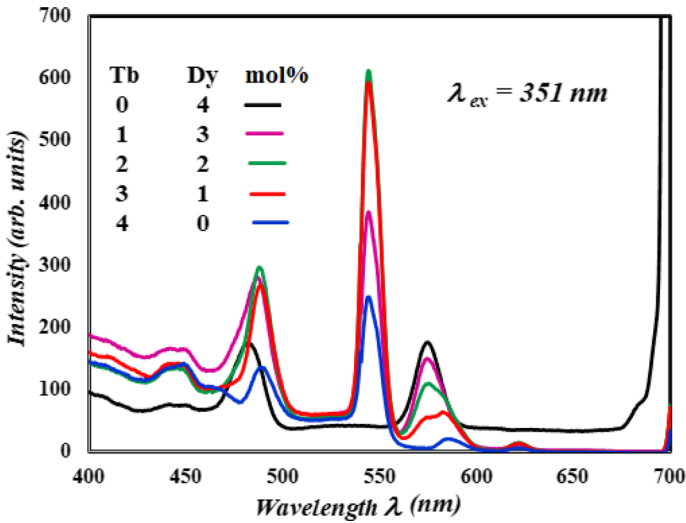


**Fig. 8** the emission for the Dy<sup>3+</sup>/Tb<sup>3+</sup> co-doped glass samples under excitation at 351 nm

$$I = I_0 + A_1 \exp\left(-\frac{t}{\tau_1}\right) + A_2 \exp\left(-\frac{t}{\tau_2}\right)$$

where  $I_0$  is the intensity at  $t=0$ , and  $I$  is intensity at time  $t$ ,  $A_1$  and  $A_2$  are the amplitudes of decay constants and  $\tau_1$  and  $\tau_2$  are the luminescence lifetimes for fast and slow channels of decay respectively. The average values of decay time are calculated by using the formula given as (Ye et al. 2023):

$$\tau_{avg} = \frac{(A_1 \tau_1^2 + A_2 \tau_2^2)}{(A_1 \tau_1 + A_2 \tau_2)}$$

The average lifetime values for Dy<sup>3+</sup> and Tb<sup>3+</sup> ions doped glass samples are inset in Table 4. It can be seen the average lifetime increases with increase in Tb<sup>3+</sup> ion concentration signifying the lifetime values of the sensitizer [Dy<sup>3+</sup>] increases while increasing the activator [Tb<sup>3+</sup>] ions concentration up to 2 mol% (Juarez-Batalla et al. 2017; Vijayakumar et al. 2018).

The experimental lifetime values of the Tb<sup>3+</sup> ions in the co-doped glass samples under study were found to be lower than the Tb<sup>3+</sup> single doped glass samples. And increasing of the Tb<sup>3+</sup> ions lifetimes value up to 2 mol% confirms the energy transfer process from Dy<sup>3+</sup> to Tb<sup>3+</sup>, also the decreases present the possible energy transfer from Tb<sup>3+</sup> to Dy<sup>3+</sup>.

The curve for the samples under study excited at 388 nm shows the sample containing 4 mol% Dy formed emission peaks at 491 nm, and 576 nm. The emission spectra formed as the excitation to the energy level <sup>4</sup>I<sub>15/2</sub>, populated through a rapid non-radiative process to a lower <sup>4</sup>F<sub>9/2</sub> level as the small energy gap  $\approx 8000 \text{ cm}^{-1}$  (Babu and Cole 2018) formed two intense emission bands at 491 nm (blue) and 576 nm (yellow) corresponding to <sup>4</sup>F<sub>9/2</sub> → <sup>6</sup>H<sub>15/2</sub> and <sup>4</sup>F<sub>9/2</sub> → <sup>6</sup>H<sub>13/2</sub> transitions, respectively.

The transition centered at 491 nm represents the magnetic dipole (MD) transition and hasn't affected the surroundings following the selection rule ( $\Delta J = 0, \pm 1$  but  $0 \rightarrow 0$ )

**Fig. 9** **a** The color coordination of glass samples exited at 351 nm. **b** Lifetime decay of Dy<sup>3+</sup> ions in glass samples exited at 351 nm. **c** Lifetime decay of Tb<sup>3+</sup> ions in glass samples exited at 351 nm

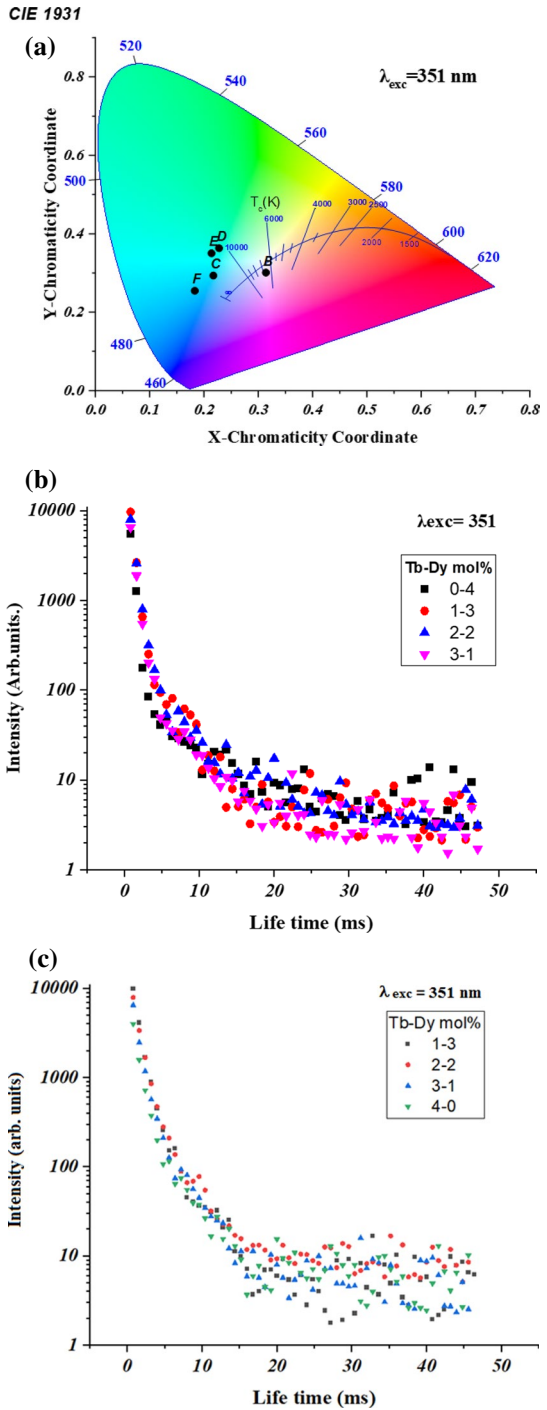


**Table 5** (A) The CIE chromaticity coordinate, green/yellow, yellow/blue ratio, lifetime decay of Dy<sup>3+</sup>, Tb<sup>3+</sup> of prepared glass samples excited at 351 nm. (B) The CIE chromaticity coordinate, green/yellow, yellow/blue ratio, lifetime decay of Dy<sup>3+</sup>, Tb<sup>3+</sup> of prepared glass samples excited at 388 nm. (C) The CIE chromaticity coordinate, green/yellow, yellow/blue ratio, lifetime decay of Dy<sup>3+</sup>, Tb<sup>3+</sup> of prepared glass samples excited at 453 nm

Sample Tb-Dy	Symbol	Color coordination (x, y)	Lifetime Dy <sup>3+</sup> ion (ms)	Lifetime Tb <sup>3+</sup> ion (ms)	Y/B	G/Y
<b>(A)</b>						
0-4	B	(0.314, 0.301)	0.5313	–	1	0.24
1-3	C	(0.217, 0.293)	0.6092	0.9994	0.53	2.6
2-2	D	(0.228, 0.364)	0.7058	1.154811	0.37	5.6
3-1	E	(0.214, 0.350)	0.6473	1.033627	0.21	10.4
4-0	F	(0.183, 0.255)	–	1.176519	0.05	31
<b>(B)</b>						
0-4	B	(0.24576, 0.26047)	0.3903	–	0.9	0.03
1-3	C	(0.25971, 0.3867)	0.5919	1.1485	0.7	2.2
2-2	D	(0.25929, 0.44324)	0.6682	1.428463	0.5	4.5
3-1	E	(0.24161, 0.42476)	0.6735	1.527974	0.3	7.3
4-0	F	(0.33459, 0.29068)	–	1.078932	0.2	14
<b>(C)</b>						
0-4	B	(0.3723, 0.61503)	0.4085	–	–	–
1-3	C	(0.34539, 0.64181)	0.6092	1.1051	–	2
2-2	D	(0.32966, 0.65457)	0.6723	1.487539	–	4.5
3-1	E	(0.50814, 0.47038)	0.6962	1.517159	–	7
4-0	F	(0.4303, 0.55244)	–	0.9404	–	–

forbidden) (Babu and Cole 2018). While the transition at 576 nm is a forced electric dipole (ED) transition, which follows ( $\Delta J=2$  and  $\Delta L=2$ ) and is hypersensitive to the ligand field environment around the Dy<sup>3+</sup> ion site. The symmetry of the Dy<sup>3+</sup> ions is responsible for the luminous emission intensity. Figure 10 observed the absence of symmetry as the difference in the intensity of yellow and blue. With the help of the ratio Y/B value, it could determine the distortion around Dy as it observed the lower symmetric sites around the Dy<sup>3+</sup> ions to the neighboring atoms, the more covalency around Dy with oxygen ligands, the more intense yellow emission than the blue emission in the photoluminescence spectrum (Ravita and Rao 2021; Rani et al. 2019; Vijayakumar et al. 2018).

The same position peak was observed in Dy after excitation with the same wavelength in a sample containing 4 mol% Tb. In addition, the peak at 543 nm. The emission spectra of Tb represent the excitation to energy level <sup>5</sup>G<sub>6</sub> to populate metastable non-radiatively to <sup>5</sup>D<sub>3</sub> and <sup>5</sup>D<sub>4</sub> excited states. The emission from level <sup>5</sup>D<sub>3</sub> is absent and replaced by only the emission from level <sup>5</sup>D<sub>4</sub> because of cross-relaxation induced by a resonance between the adjacent Tb<sup>3+</sup> ions, which can be described by the following equation: <sup>5</sup>D<sub>3</sub> + <sup>7</sup>F<sub>6</sub> → <sup>5</sup>D<sub>4</sub> + <sup>7</sup>F<sub>0</sub> and <sup>5</sup>D<sub>3</sub> + <sup>7</sup>F<sub>6</sub> → <sup>7</sup>F<sub>0</sub> + <sup>5</sup>D<sub>4</sub> (Zhao et al. 2013; Quang et al. 2020; Dillip et al. 2016). The emission peak at 543 nm represents the <sup>5</sup>D<sub>4</sub> → <sup>7</sup>F<sub>5</sub> transition with a prominent green light. It is a magnetic-dipole transition that follows the selection rule of  $J = \pm 1$ .

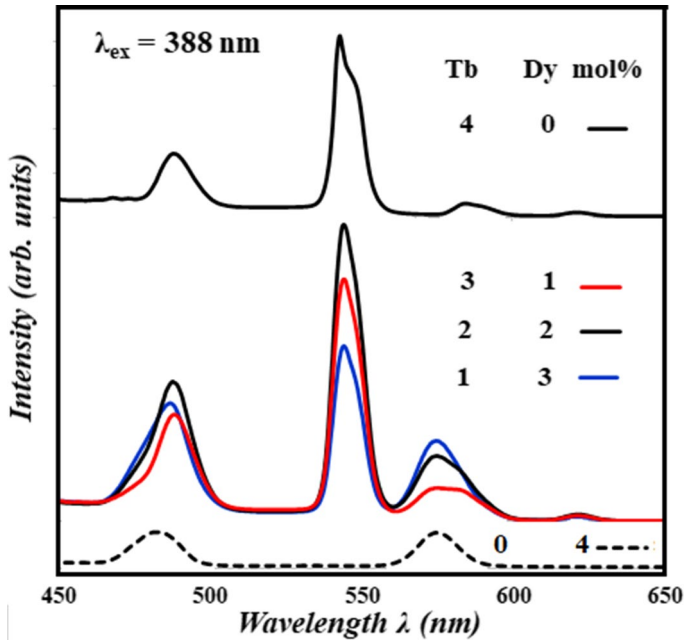


**Fig. 10** the emission for the Dy<sup>3+</sup>/Tb<sup>3+</sup> co-doped glass samples under excitation at 388 nm

The other emission bands centered at 491 nm and 576 nm are attributed to the electronic transitions  $^5D_4 \rightarrow ^7F_J$  ( $J=6, 4$ ) (Zhao et al. 2013; Zur et al. 2018). The intensity ratio (blue to green) describes the irregular behavior of doping ions in the host, for all terbium doped glasses, as it explains the ratio Y/B for Dy (Ravita and Rao 2021).

The CIE 1931 color chromaticity and lifetime decay for Dy<sup>3+</sup> and Tb<sup>3+</sup> excited at 388 nm are shown in Fig. 11a, b and c, respectively.

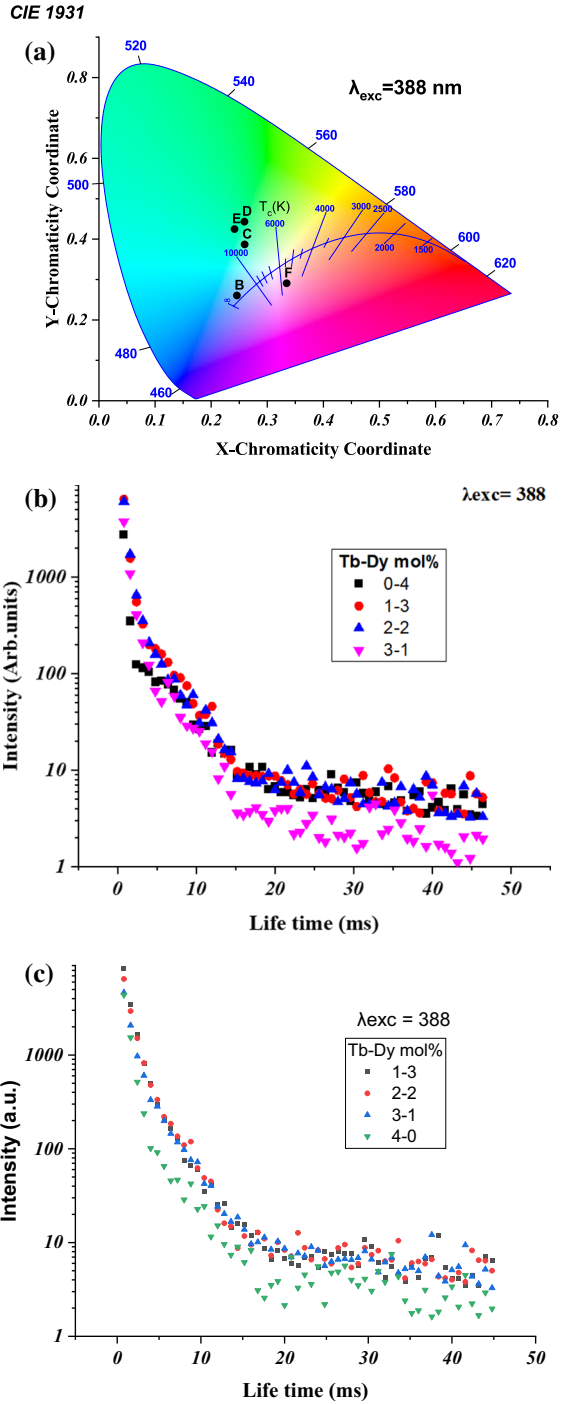
The coordination of glass samples excited at 388B. and lifetime determined and tabulated in Table 5B.

The curve for the sample containing 4 mol% Dy or Tb or both excited at 453 nm shows the sample containing 4 mol% Dy formed emission peaks at 576 nm (Fig. 12). The emission spectra formed as the excitation to the energy level  $^4I_{15/2}$ , populated through a rapid non-radiative process to a lower  $^4F_{9/2}$  level as the small energy gap  $\approx 8000 \text{ cm}^{-1}$  (Babu and Cole 2018) formed intense emission bands at 576 nm (yellow) corresponding to  $^4F_{9/2} \rightarrow ^6H_{15/2}$  transitions.

The transition centered at 491 nm represents the magnetic dipole (MD) transition and hasn't affected the surroundings following the selection rule ( $\Delta J=0, \pm 1$  but  $0 \rightarrow 0$  forbidden) (Babu and Cole 2018). While the transition at 576 nm is a forced electric dipole (ED) transition, which follows ( $\Delta J=2$  and  $\Delta L=2$ ) and is hypersensitive to the ligand field environment around the Dy<sup>3+</sup> ion site. The symmetry of the Dy<sup>3+</sup> ions is responsible for the luminous emission intensity. Figure 12 observed the absence of symmetry as the difference in the intensity of yellow and blue. With the help of the ratio Y/B value, it could determine the distortion around Dy as it observed the lower symmetric sites around the Dy<sup>3+</sup> ions to the neighboring atoms, the more covalency around Dy with oxygen ligands, the more



**Fig. 11** **a** The color coordination of glass samples exited at 388 nm. **b** Lifetime decay of Dy<sup>3+</sup> ions in glass samples exited at 388 nm. **c** Lifetime decay of Tb<sup>3+</sup> ions in glass samples exited at 388 nm



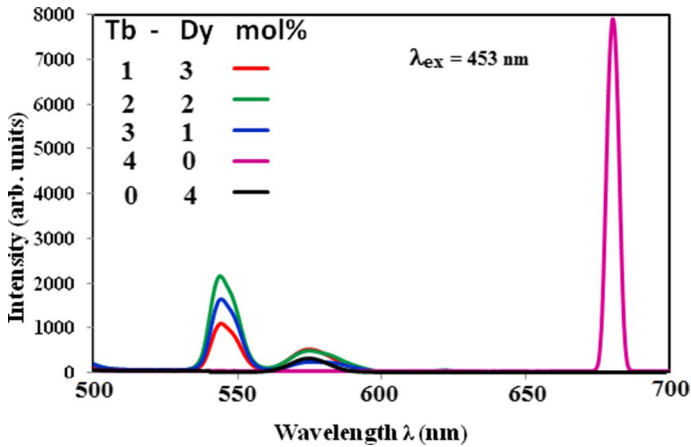


**Fig. 12** the emission for the  $\text{Dy}^{3+}/\text{Tb}^{3+}$  co-doped glass samples under excitation at 453 nm

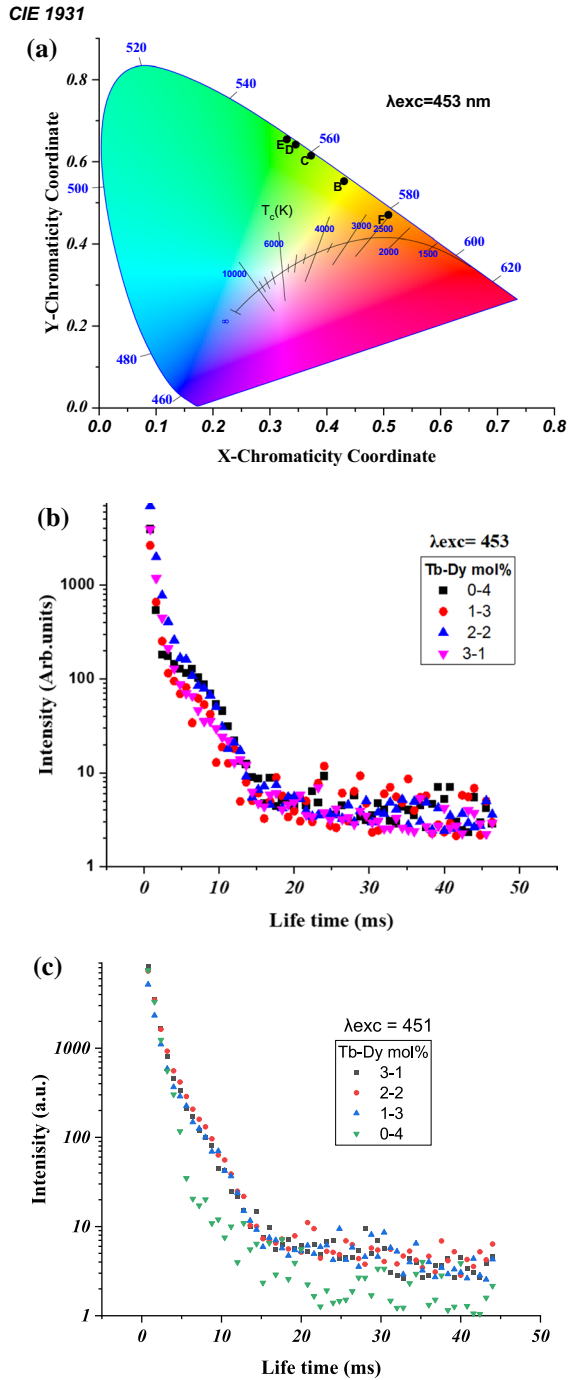
intense yellow emission than the blue emission in the photoluminescence spectrum (Ravita and Rao 2021; Rani et al. 2019; Vijayakumar et al. 2018).

The CIE 1931 color chromaticity and lifetime decay for  $\text{Dy}^{3+}$  and  $\text{Tb}^{3+}$  excited at 388 nm are shown in Fig. 13a, b and c, respectively. The coordination of glass samples excited at 453 nm, and lifetime determined and tabulated in Table 5C.

## 4 Conclusion

Glass samples of bismuth gallium germanium borosilicate containing  $\text{Tb}_4\text{O}_7$  and  $\text{Dy}_2\text{O}_3$  were prepared using the melt quenching process. At 1270 nm, the  ${}^6\text{H}_{15/2}$ ,  ${}^6\text{F}_{11/2}$  +  ${}^6\text{H}_{9/2}$  transitions have the highest strong absorption in the glasses' UV-Vis NIR. When the samples are excited at 351, 388 and 453 nm the emission spectra include  $\text{Dy}^{3+}$  and  $\text{Tb}^{3+}$  emission. This clearly indicates the energy transfer from the  $\text{Dy}^{3+}$  to the  $\text{Tb}^{3+}$  ions. And the lifetime decay confirmed this transfer. The sample containing equal ratio between two rare earth ions is the best energy transfer condition. After this concentration ( $\text{Tb}^{3+}$  greater than 2 mol%) the energy transfer from  $\text{Tb}^{3+}$  to  $\text{Dy}^{3+}$  in sample excited at 351 nm. After doping with  $\text{Dy}^{3+}$ , the prepared glasses emit yellow and blue emissions, with a white light overall. The decreased emission of  $\text{Dy}^{3+}$  and the increased emission of  $\text{Tb}^{3+}$  were reported as evidence of energy transfer in the glasses.

**Fig. 13** **a** The color coordination of glass samples exited at 453 nm. **b** lifetime decay of Dy<sup>3+</sup> ions in glass samples exited at 453 nm. **c** Lifetime decay of Tb<sup>3+</sup> ions in glass samples exited at 453 nm



**Author contributions** IK and AR have proposed the idea. Material preparation, experimental measurements, data collection and analysis were performed by IK and AR. The first draft of the manuscript was written by AR. IK and AR commented on previous versions of the manuscript and approved the final manuscript.

**Funding** Open access funding provided by The Science, Technology & Innovation Funding Authority (STDF) in cooperation with The Egyptian Knowledge Bank (EKB). No funding for research.

**Availability of data and materials** The data that support the findings of this study are available from the corresponding author upon reasonable request.

## Declarations

**Competing interests** The authors declare that they have no known competing financial interests or personal relationships that could have appeared to influence the work reported in this paper.

**Ethics approval** This paper meets the ethical standards of this journal.

**Consent to participate** All authors agree with the review of this paper in this journal.

**Open Access** This article is licensed under a Creative Commons Attribution 4.0 International License, which permits use, sharing, adaptation, distribution and reproduction in any medium or format, as long as you give appropriate credit to the original author(s) and the source, provide a link to the Creative Commons licence, and indicate if changes were made. The images or other third party material in this article are included in the article's Creative Commons licence, unless indicated otherwise in a credit line to the material. If material is not included in the article's Creative Commons licence and your intended use is not permitted by statutory regulation or exceeds the permitted use, you will need to obtain permission directly from the copyright holder. To view a copy of this licence, visit <http://creativecommons.org/licenses/by/4.0/>.

## References

- Aljewaw, O.B., Abdul Karim, M.K., Kamari, H.M., Zaid, M.H.M., Noor, N.M., Isa, I.N.C., Abu Mhareb, M.H.: Impact of Dy<sub>2</sub>O<sub>3</sub> substitution on the physical, structural and optical properties of lithium–aluminum–borate glass system. *Appl. Sci.* **10**(22), 1–17 (2020). <https://doi.org/10.3390/app10228183>
- Babu, K.V., Cole, S.: Luminescence properties of Dy<sup>3+</sup>-doped alkali lead aluminoborosilicate glasses. *Ceram. Int.* **44**(8), 9080–9090 (2018). <https://doi.org/10.1016/j.ceramint.2018.02.115>
- Babu, S., Prasad, V.R., Rajesh, D., Ratnakaram, Y.C.: Luminescence properties of Dy<sup>3+</sup> doped different fluoro-phosphate glasses for solid state lighting applications. *J. Mol. Struct.* **1080**, 153–161 (2015). <https://doi.org/10.1016/j.molstruc.2014.09.080>
- Bahadur, A., Yadav, R.S., Yadav, R.V., Rai, S.B.: Multimodal emissions from Tb<sup>3+</sup>/Yb<sup>3+</sup> co-doped lithium borate glass: Upconversion, downshifting and quantum cutting. *J. Solid State Chem.* **246**(11), 81–86 (2017). <https://doi.org/10.1016/j.jssc.2016.11.004>
- Bashar, K.A., Fong, W.L., Haider, K.A., Baki, S.O., Zaid, M.H.M., Mahdi, M.A.: Optical studies on Tb<sup>3+</sup>:Dy<sup>3+</sup> singly and doubly doped Borosilicate glasses for white light and solid state lighting applications. *J. Noncryst. Solids* **534**(11), 119943 (2020). <https://doi.org/10.1016/j.jnoncrysol.2020.119943>
- Carreira, J.F.C., Sava, B.A., Boroica, L., Elisa, M., Stefan, R., Monteiro, R.C.C., Monteiro, T., Rino, L.: Structural and luminescence characterization of a Dy/Tb co-doped borophosphate glass. *J. Noncryst. Solids* **526**(10), 119719 (2019). <https://doi.org/10.1016/j.jnoncrysol.2019.119719>
- Chen, Q., Wang, H., Wang, G., Yin, S.: Magneto optical properties of rare earth Tb<sub>2</sub>O<sub>3</sub> doped PbO–Bi<sub>2</sub>O<sub>3</sub>–B<sub>2</sub>O<sub>3</sub> glass. *J. Non. Cryst. Solids* **470**(5), 99–107 (2017). <https://doi.org/10.1016/j.jnoncrysol.2017.05.008>
- Dharmaiah, P., Viswanath, C.S.D., Basavapoornima, Ch., Krishnaiah, K.V., Jayasankar, C.K., Hong, S.-J.: Luminescence and energy transfer in Dy<sup>3+</sup>/Tb<sup>3+</sup> co-doped transparent oxyfluorosilicate glass-ceramics for green emitting applications. *Mater. Res. Bull.* **83**, 507–514 (2016). <https://doi.org/10.1016/j.materresbull.2016.06.044>
- Dillip, G.R., Reddy, C.M., Rajesh, M., Chaurasia, S., Raju, B.D.P., Joo, S.W.: Green fluorescence of terbium ions in lithium fluoroborate glasses for fibre lasers and display devices. *Bull. Mater. Sci.* **39**(3), 711–717 (2016). <https://doi.org/10.1007/s12034-016-1192-0>

- Divina, R., Teresa, P.E., Marimuthu, K.: Dy<sup>3+</sup> ion as optical probe to study the luminescence behavior of Alkali lead bismuth borate glasses for w-LED application. *J. Alloys Compd.* **883**, 160845 (2021). <https://doi.org/10.1016/j.jallcom.2021.160845>
- Gökçe, M., Koçyiğit, D.: Spectroscopic investigations of Dy<sup>3+</sup> doped borogermanate glasses for laser and wLED applications. *Opt. Mater. (amst)* **89**(2), 568–575 (2019). <https://doi.org/10.1016/j.optmat.2019.02.004>
- Guo, H., Wang, Y., Gong, Y., Yin, H., Mo, Z., Tang, Y., Chi, L.: Optical band gap and photoluminescence in heavily Tb<sup>3+</sup> doped GeO<sub>2</sub>-B<sub>2</sub>O<sub>3</sub>-SiO<sub>2</sub>-Ga<sub>2</sub>O<sub>3</sub> magneto-optical glasses. *J. Alloys Compd.* **686**, 635–640 (2016). <https://doi.org/10.1016/j.jallcom.2016.06.074>
- Hegde, V., Dwaraka, C.S., Mahato, V.K.K., Kamath, S.D.: Warm white light and colour tunable characteristics of Dy<sup>3+</sup> co-doped with Eu<sup>3+</sup> and Pr<sup>3+</sup> zinc sodium bismuth borate glasses for solid state lighting applications. *Mater. Chem. Phys.* **234**(5), 369–377 (2019). <https://doi.org/10.1016/j.matchemphys.2019.05.063>
- Ichoja, A., Hashim, S., Ghoshal, S.K.: Judd–Ofelt calculations for spectroscopic characteristics of Dy<sup>3+</sup>-activated strontium magnesium borate glass. *Optik (stuttg)* **218**(5), 165001 (2020). <https://doi.org/10.1016/j.ijleo.2020.165001>
- Juarez-Batalla, J., Meza-Rocha, A.N., Munoz, G.H., Caldino, U.: Green to white tunable light emitting phosphors: Dy<sup>3+</sup>/Tb<sup>3+</sup> in zinc phosphate glasses. *Opt. Mater. (amst.)* **64**, 33–39 (2017). <https://doi.org/10.1016/j.optmat.2016.11.033>
- Karki, S., Kesavulu, C.R., Kim, H.J., Kaewkhao, J., Chanthima, N., Kothan, S., Kaewjaeng, S.: Physical, optical and luminescence properties of the Dy<sup>3+</sup> doped barium borophosphate glasses. *J. Noncryst. Solids* **521**, 119483 (2019)
- Kashif, I., Ratep, A.: Judd–Ofelt and luminescence study of Dysprosium-doped lithium borosilicate glasses for lasers and w-LEDs. *Bol. Soc. Esp. Ceram. Vidr.* **61**, 1–12 (2021). <https://doi.org/10.1016/j.bsecev.2021.06.001>
- Kashif, I., Ratep, A.: Cool white light emission from Dy<sup>3+</sup>-doped SiO<sub>2</sub>-Bi<sub>2</sub>O<sub>3</sub>-Ga<sub>2</sub>O<sub>3</sub>-B<sub>2</sub>O<sub>3</sub>-GeO<sub>2</sub>-TeO<sub>2</sub> glasses: structural and spectroscopic properties. *Mater. Sci. Eng. B* **275**(12), 115488 (2022a). <https://doi.org/10.1016/j.mseb.2021.115488>
- Kashif, I., Ratep, A.: Effect of addition of dysprosium oxide on spectroscopic properties and Judd–Ofelt analysis of lithium borosilicate glass system. *SILICON* (2022b). <https://doi.org/10.1007/s12633-022-02249-7>
- Kaur, S., Deopa, N., Prasad, A., Bajaj, R., Rao, A.S.: Intense green emission from Tb<sup>3+</sup> ions doped zinc lead alumino borate glasses for laser and w-LEDs applications. *Opt. Mater. (Amst.)* **84**(5), 318–323 (2018). <https://doi.org/10.1016/j.optmat.2018.07.020>
- Kesavulu, C.R., Jayasankar, C.K.: White light emission in Dy<sup>3+</sup>-doped lead fluorophosphate glasses. *Mater. Chem. Phys.* **130**(3), 1078–1085 (2011). <https://doi.org/10.1016/j.matchemphys.2011.08.037>
- Kumar, M., Rao, A.S.: Influence of Tb<sup>3+</sup> ions concentration and temperature on lithium bismuth alumino borosilicate glasses for green photonic device applications. *Opt. Mater. (amst)* **120**(8), 111439 (2021). <https://doi.org/10.1016/j.optmat.2021.111439>
- Ma, Y., Zhao, G., Guo, Y., Hou, J., Liu, Y., Zhou, Y., Zou, J., Fang, Y.: Structural characterization and photoluminescence properties of B<sub>2</sub>O<sub>3</sub>-Bi<sub>2</sub>O<sub>3</sub>-SiO<sub>2</sub> glass containing Dy<sup>3+</sup> ions. *J. Lumin.* **227**(5), 117591 (2020). <https://doi.org/10.1016/j.jlumin.2020.117591>
- Ma, J., Sun, Y., Yu, F., Xue, T., Hu, L.: Boosting visible luminescence of Tb<sup>3+</sup>-activated ZBLAN fluoride glasses by Dy<sup>3+</sup> co-doping. *J. Lumin.* **238**(3), 118247 (2021). <https://doi.org/10.1016/j.jlumin.2021.118247>
- Mariselvam, K., Liu, J.: Down-conversion luminescence and shielding parameters of Dy<sup>3+</sup>: NFBT glass for white LED and radiation applications. *Opt. Mater. (amst.)* **114**(2), 110997 (2021). <https://doi.org/10.1016/j.optmat.2021.110997>
- Mariyappan, M., Arunkumar, S., Marimuthu, K.: Effect of Bi<sub>2</sub>O<sub>3</sub> on the structural and spectroscopic properties of Sm<sup>3+</sup> ions doped sodiumfluoroborate glasses. *J. Mol. Struct.* **1105**, 214–224 (2016). <https://doi.org/10.1016/j.molstruc.2015.10.043>
- Pisarska, J., Kos, A., Pietrasik, E., Pisarski, W.A.: Energy transfer from Dy<sup>3+</sup> to Tb<sup>3+</sup> in lead borate glass. *Mater. Lett.* **129**, 146–148 (2014). <https://doi.org/10.1016/j.matlet.2014.05.035>
- Quang, V.X., Do, P.V., Ca, N.X., Thanh, L.D., Tuyen, V.P., Tan, P.M., Hoa, V.X., Hien, N.T.: Role of modifier ion radius in luminescence enhancement from 5D<sub>4</sub> level of Tb<sup>3+</sup> ion doped alkali-alumino-telluroborate glasses. *J. Lumin.* **221**(1), 117039 (2020). <https://doi.org/10.1016/j.jlumin.2020.117039>
- Ramachari, D., Moorthy, L.R., Jayasankar, C.K.: Energy transfer and photoluminescence properties of Dy<sup>3+</sup>/Tb<sup>3+</sup> co-doped oxyfluorosilicate glass-ceramics for solid-state white lighting. *Ceram. Int.* **40**(7), 11115–11121 (2014). <https://doi.org/10.1016/j.ceramint.2014.03.136>

- Rani, P.R., Venkateswarlu, M., Mahamuda, S., Swapna, K., Deopa, N., Rao, A.S.: Spectroscopic studies of Dy<sup>3+</sup> ions doped barium lead alumino fluoro borate glasses. *J. Alloys Compd.* **787**, 503–518 (2019). <https://doi.org/10.1016/j.jallcom.2019.02.088>
- Rao, M.S., Sudarsan, V., Brik, M.G., Gandhi, Y., Bhargavi, K., Piasecki, M., Kityk, I.V., Veeraiiah, N.: De-quenching influence of aluminum ions on Y/B ratio of Dy<sup>3+</sup> ions in lead silicate glass matrix. *J. Alloys Compd.* **575**, 375–381 (2013). <https://doi.org/10.1016/j.jallcom.2013.05.098>
- Ravita, Rao, A.S.: Effective energy transfer from Dy<sup>3+</sup> to Tb<sup>3+</sup> ions in thermally stable KZABS glasses for intense green emitting device applications. *J. Lumin.* **239**(7), 118325 (2021). <https://doi.org/10.1016/j.jlumin.2021.118325>
- Sales, T.O., Amjad, R.J., Jacinto, C., Dousti, M.R.: Concentration dependent luminescence and cross-relaxation energy transfers in Tb<sup>3+</sup> doped fluoroborate glasses. *J. Lumin.* **205**(9), 282–286 (2019). <https://doi.org/10.1016/j.jlumin.2018.09.031>
- Selvi, S., Venkataiah, G., Arunkumar, S., Muralidharan, G., Marimuthu, K.: Structural and luminescence studies on Dy<sup>3+</sup> doped lead boro-telluro-phosphate glasses. *Phys. B Condens. Matter* **454**, 72–81 (2014). <https://doi.org/10.1016/j.physb.2014.07.018>
- Shaaban, K.H.S., El-Maaref, A.A., Abdelawwad, M., Saddeek, Y.B., Wilke, H., Hillmer, H.: Spectroscopic properties and Judd–Ofelt analysis of Dy<sup>3+</sup> ions in molybdenum borosilicate glasses. *J. Lumin.* **196**(12), 477–484 (2018). <https://doi.org/10.1016/j.jlumin.2017.12.041>
- Sun, X.-Y., Gu, M., Huang, S.-M., Liu, X.-L., Liu, B., Ni, C.: Enhancement of Tb<sup>3+</sup> emission by non-radiative energy transfer from Dy<sup>3+</sup> in silicate glass. *Phys. B Condens. Matter* **404**(1), 111–114 (2009). <https://doi.org/10.1016/j.physb.2008.10.039>
- Sun, X., Huang, S., Gong, X., Gao, Q., Ye, Z., Cao, C.: Spectroscopic properties and simulation of white-light in Dy<sup>3+</sup>-doped silicate glass. *J. Non-Cryst. Solids* **356**(2), 98–101 (2010)
- Swapna, K., Mahamuda, S., Srinivasa Rao, A., Jayasimhadri, M., Sasikala, T., Rama Moorthy, L.: Visible fluorescence characteristics of Dy<sup>3+</sup> doped zinc alumino bismuth borate glasses for optoelectronic devices. *Ceram. Int.* **39**(7), 8459–8465 (2013). <https://doi.org/10.1016/j.ceramint.2013.04.028>
- Vijayakumar, R., Venkataiah, G., Marimuthu, K.: Structural and luminescence studies on Dy<sup>3+</sup> doped borophosphate glasses for white LED's and laser applications. *J. Alloys Compd.* **652**, 234–243 (2015). <https://doi.org/10.1016/j.jallcom.2015.08.219>
- Vijayakumar, M., Viswanathan, K., Marimuthu, K.: Structural and optical studies on Dy<sup>3+</sup>:Tb<sup>3+</sup> co-doped zinc leadfluoro-borophosphate glasses for white light applications. *J. Alloys Compd.* **745**, 306–318 (2018). <https://doi.org/10.1016/j.jallcom.2018.02.211>
- Wang, L., Guo, Z., Wang, S., Zhang, H., Lv, H., Wang, T., Su, C.: Luminescence properties of Dy<sup>3+</sup> doped glass ceramics containing Na<sub>3</sub>Gd(PO<sub>4</sub>)<sub>2</sub>. *J. Noncryst. Solids* **543**(5), 120091 (2020). <https://doi.org/10.1016/j.jnoncrsol.2020.120091>
- Yang, H., Zhu, Z.: Magneto-optical glass mixed with Tb<sup>3+</sup> ions: High Verdet constant and luminescence properties. *J. Lumin.* **231** (10), 117804 (2021)
- Ye, G., Fang, L., Zhou, X., Xia, H., Song, H., Chen, B.: Tunable luminescence and energy transfer properties in novel fluoro-oxide glass ceramics containing KGd<sub>2</sub>F<sub>7</sub>:Dy<sup>3+</sup>/Tb<sup>3+</sup> nanocrystals. *Mater. Res. Bull.* **157**, 112028 (2023)
- Zaman, F., Srisittipokakun, N., Rooh, G., Khattak, S.A., Kaewkhao, J., Rani, M., Kim, H.J.: Comparative study of Dy<sup>3+</sup> doped borate glasses on the basis of luminescence and lasing properties for white-light generation. *Opt. Mater. (amst)* **119**(6), 111308 (2021). <https://doi.org/10.1016/j.optmat.2021.111308>
- Zhang, H., Lin, P.J., Yuan, J.L., Pun, E.Y.B., Li, D.S., Lin, H.: Multiplier effect of sensitization for Dy<sup>3+</sup> fluorescence in borosilicate glass phosphor. *J. Lumin.* **221**(9), 2019 (2020). <https://doi.org/10.1016/j.jlumin.2020.117062>
- Zhao, Y.G., Shi, D.M., Wang, X.F., Liu, J.: Role of B<sub>2</sub>O<sub>3</sub> substitution by SiO<sub>2</sub> on luminescence properties of Tb<sup>3+</sup>-doped SiO<sub>2</sub>-B<sub>2</sub>O<sub>3</sub>-Na<sub>2</sub>O-BaO glass. *Phys. Procedia*, **48**, 165–171 (2013)
- Zur, L., Kos, A., Gorny, A., Sołtys, M., Pietrasik, E., Pisarska, J., Goryczka, T., Pisarski, W.A.: Influence of acceptor concentration on crystallization behavior and luminescence properties of lead borate glasses co-doped with Dy<sup>3+</sup> and Tb<sup>3+</sup> ions. *J. Alloys Compd.* **749**, 561–566 (2018). <https://doi.org/10.1016/j.jallcom.2018.03.282>